# Model Correlation and Thermal Analysis of xEMU Boot at Lunar South Pole Temperatures

Emma Quick[1]
*Amentum, 2224 Bay Area Blvd, Houston, Texas, 77058*

Noah L. Andersen[2]
*HX5, LLC, 2224 Bay Area Blvd, Houston, TX, 77058*

Ben Swartout[3]
*NASA Johnson Space Center, Houston, TX, 77058*

Shane McFarland[4]
*Aegis Aerospace / KBR HHPC / NASA Johnson Space Center, Houston, TX, 77058*

**The National Aeronautics and Space Administration (NASA) Artemis program plans to send astronauts to the lunar south pole, a region of the moon that is colder than previous lunar missions and low earth orbit operations. The spacesuit boots that will be used on these missions will be directly impacted by these extremely cold temperatures (down to ~50 K). To assess the performance of the Exploration Extravehicular Mobility Unit (xEMU) lunar boot in these extreme temperatures, the boot was tested at the Jet Propulsion Lab (JPL) in the Cryogenic Ice Transfer, Acquisition Development, and Excavation Laboratory (CITADEL) thermal vacuum (TVAC) chamber. This data was used to correlate thermal models to predict operational performance of the boots on the lunar south pole. This paper documents the data analysis, thermal boot model correlation, and operational predictions conducted using data from the xEMU TVAC test. Data from the test series was used to determine expected thermal conductances within the boot and between the boot and environment. These conductances were used to correlate a Thermal Desktop model of the xEMU boot across 10 different test points which varied external temperature, internal boot ventilation flowrate, and contact pressure. The correlated model was then used to predict operational performance in the lunar south pole. While the predictions indicate promising evidence for performance of the boots at the 100K test point, there is still substantial uncertainty in performance, particularly at the 48K test point. The results of this test series and model correlation stress the importance of improved testing for characterizing the expected thermal resistance between the outside of the boot and the lunar surface.**

## Acronyms and Nomenclature

| | | |
|---|---|---|
| $A_{contact}$ | = | surface area of contact |
| AI | = | Artificial Intelligence |
| CAD | = | Computer-Aided Design |

---

[1] Chemical Engineer – Modeling & Simulations, Thermal & Life Support Systems Analysis, JETSII.
[2] Thermal Analysis Engineer, Thermal & Life Support Systems Analysis, JETSII.
[3] Spacesuit Engineer, Spacesuit and Crew Survival Systems Branch, 2101 E NASA Parkway, Mail Code EC5
[4] Advanced Suit Team Deputy Lead for Technology Development, Spacesuit and Crew Survival Systems Branch, 2101 E NASA Parkway, Mail Code EC5



***Artificial Intelligence (AI) Usage Disclosure***
*This document was created with assistance from Microsoft 365 Copilot for rephrasing and keeping content succinct. The content has been reviewed and edited by Emma Quick. More information on the extent and nature of AI usage is included in the Acknowledgements sections of the document.*

| | | |
|---|---|---|
| $C_{conduction}$ | = | conduction coefficient |
| CITADEL | = | Cryogenic Ice Transfer, Acquisition Development, and Excavation Laboratory |
| DVT | = | Design-Verification-Test |
| EMU | = | Extravehicular Mobility Unit |
| EPG | = | Environmental Protection Garment |
| EVA | = | Extravehicular Activity |
| IVA | = | Intravehicular Activity |
| JPL | = | Jet Propulsion Laboratory |
| $K$ | = | scaling factor to weight model accuracy toward heat leak values |
| $k_{screw}$ | = | conductivity of a screw |
| LEO | = | lower Earth orbit |
| MLI | = | Multi-Layer Insulation |
| $N$ | = | number of steady state test points (10) |
| NASA | = | National Aeronautics and Space Administration |
| $N_{screws}$ | = | number of screws |
| $OBJECT$ | = | function to minimize with SOLVER during model correlation |
| PSR | = | Permanently Shadowed Region |
| $q_{model,i}$ | = | model-predicted heat leak at location $i$ |
| $q_{test,i}$ | = | experimental heat leak at location $i$ |
| $RMSE$ | = | root-mean-square error |
| SLI | = | Single-Layer Insulation |
| TC | = | thermocouple |
| TD | = | Thermal Desktop |
| $T_{model,i}$ | = | model-predicted temperature at location $i$ |
| $T_{test,i}$ | = | experimental temperature at location $i$ |
| TVAC | = | thermal vacuum |
| xEMU | = | Exploration Extravehicular Mobility Unit |
| .stp | = | STEP or STP file format |

# I. Introduction

A cryogenic thermal vacuum (TVAC) test was conducted within the Cryogenic Ice Transfer, Acquisition Development, and Excavation Laboratory (CITADEL) Chamber at the Jet Propulsion Laboratory (JPL) to simulate environmental conditions representative of the lunar south pole. The test article for this evaluation was a Design-Verification-Test (DVT) fidelity boot, developed as the government reference design under the Exploration Extravehicular Mobility Unit (xEMU) project.

This test campaign utilized a single boot test article, as that was what the test schedule and budget could support. Future testing may include additional boot sizes and types (lunar/LEO/Martian). An instrumented thermal manikin foot was placed inside the boot to simulate a crewmember's foot, enabling the measurement of resultant heat loads and skin temperatures. Results from this test campaign were used to correlate a Thermal Desktop (TD) model of the boot. Predicted performances of the boot in lunar permanently shadowed regions (PSRs) were also characterized.

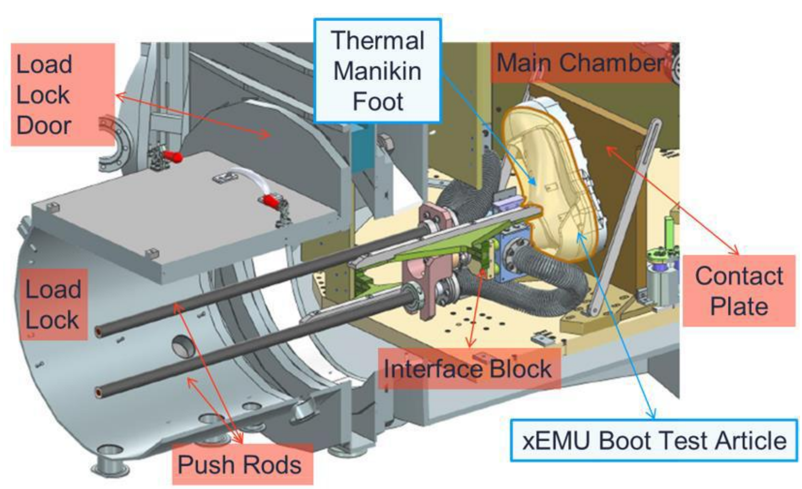

**Figure 1. Spacesuit Boot Test System Diagram.**

# II. Test Setup

This test campaign utilized a DVT-fidelity xEMU lunar spacesuit boot for thermal vacuum testing at JPL's CITADEL chamber to replicate lunar permanently shadowed region (PSR) conditions. The boot was instrumented with 56 external and 16 internal type-T thermocouples, along with six environment coupons, each equipped with thermocouples on both sides. Thermocouples were arranged in "stacks" across multiple layers (e.g., bladder, restraint, frame, thermal insert, outsole) that were aligned normally to the surface of the foot. Internally, a thermal manikin foot with water loops maintained a constant boundary temperature representative of crew skin temperature and included temperature and heat flux sensors at 16 discrete locations on the foot.

The boot was mounted on an actuated push-rod system enabling transfer from the thermally neutral load lock to the conditioned vacuum chamber, simulating the intravehicular activity (IVA) to extravehicular activity (EVA) transition expected during Artemis III. Inside the chamber, a miniature thermal shroud (hereafter "MiniShroud") provided localized thermal conditioning, and a thermally controlled stomp pad simulated contact with the lunar surface. The boot was pressurized to 29.65 kPa (4.3 psia) with ventilation flow at 12.4 SLPM (1.5 ACFM) which represents one fourth of the total ventilation flowrate expected to the suit (flow is picked up in arms and boots, so an anticipated 25% of the flow will go to the boot). Additional details on the test setup are provided in *xEMU Spacesuit Boot Lunar South Pole Thermal Vacuum Testing* [1].

Test parameters included ventilation flow rate, contact versus radiation environments, foot contact pressure, manikin foot temperature setpoint, and test duration. For model correlation, runs were performed until thermal steady state was achieved, defined as less than 1 °C change per hour across most of the ~80 thermocouples. Early data points were evaluated and found to not reach steady state. These trials were excluded from the dataset used to correlate the model.

## III. Correlation

The xEMU boot model was developed prior to testing and relied on numerous assumptions. Correlating the model to test data allowed several of these assumptions to be relaxed, verified, or updated. This section contains detailed information on the thermal models and the process of correlating them to test data.

### A. Model Description

The thermal model was developed using Thermal Desktop and a FORTRAN based human foot model. The original boot model was developed using SINDA/FLUINT for the Extravehicular Mobility Unit (EMU) in 1979 [2]. Since then it has been iterated and improved numerous times [3] [4] [5] [6] [7] [8] [9]. The description of the model is broken into two sections: the MiniShroud and the boot. While the boot portion of the model has an extensive history, the MiniShroud portion of the model was developed specifically for this test series.

### B. Mini Shroud Model

The MiniShroud portion of the thermal model was developed to capture the influence of the MiniShroud on boot's surrounding environmental temperatures. This chamber geometry was based on the latest Computer-Aided Design (CAD) model of the MiniShroud fabricated at JPL for this test series. The thermal model incorporates key components, including the stomp pad, copper bars mounted to its rear surface, Teflon fabric cutouts adhered to the stomp pad, the enclosure's top, sides, and bottom panels, and the single-layer insulation (SLI) curtain positioned between the boot and the load lock. Figure 2 compares the thermal model geometry with the original CAD (.stp) file, illustrating interior and rear views of both representations.

To simulate the surrounding chamber environment, five sink temperature nodes were placed around each face of the MiniShroud, except the rear face where the copper bars served as the thermal sink. All chamber walls were modeled as insulated to capture the effect of the physical insulation applied to the outside of the MiniShroud.

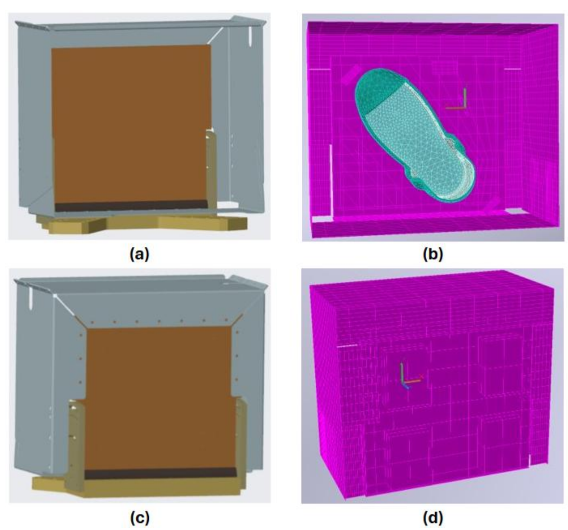


**Figure 2. Comparison of CAD file (.stp) and Thermal Desktop (TD) geometry. (a) CAD interior, (b) TD interior, (c) back of CAD, (d) back of TD.**

During correlation, these sink temperatures were iteratively adjusted using Thermal Desktop's SOLVER function until predicted temperatures aligned with test measurements. Solving for sink temperatures was required since there were no TCs placed outside the MiniShroud. The CAD also included a G10 spacer between the stomp plate and the MiniShroud base, intended to thermally isolate the stomp plate. This spacer was not explicitly modeled; instead, a gap was left between the stomp plate and the bottom of the chamber and a low-conductance contactor between these surfaces modeled the small amount of heat transfer through the spacer. SOLVER was also used to determine the appropriate conductance value for this heat transfer, and its impact is discussed in the next section.

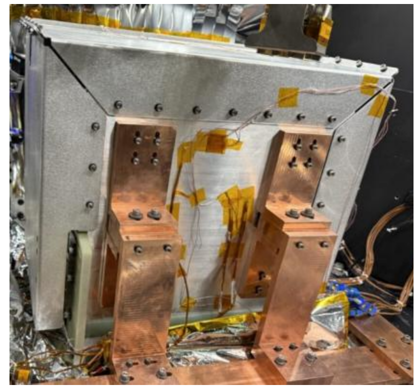

**Figure 3. Back of MiniShroud.**

Accurate representation of thermal connections between components was critical for model fidelity. The walls of the MiniShroud did not experience direct contact with the cold sink copper bars, which is the primary reason the MiniShroud did not get as cold as desired during testing. The copper bars were bolted to the stomp pad using 16 screws arranged in square patterns at each end. The stomp pad was bolted to the MiniShroud's top and side walls via three flaps. The bottom surface was attached to the walls by a single screw on either side, and the top surface was attached to the walls by three screws on each side. Figure 3 shows most of these connections. In Thermal Desktop, these mechanical joints were modeled using face and edge contactors. Conduction coefficients were calculated as follows based on contact area, material properties and quantities of screws.

$$C_{conduction} = \frac{N_{screws} \cdot k_{screw}}{A_{contact}} \tag{1}$$

where $C_{conduction}$ is the conduction coefficient (required input in Thermal Desktop), $N_{screws}$ is the number of screws, $k_{screw}$ is the conductivity of one screw, and $A_{contact}$ is the contact area of the two surfaces. Screw conductivities were derived from the *Spacecraft Thermal Control Handbook* [10] either directly or via extrapolation. The most important thermal contacts within the model are listed in following table.

**Table 1. Critical thermal contacts within the MiniShroud model.**

| From | To | Description |
|---|---|---|
| Copper Bars | Stomp Pad | Face Contactors |
| Stomp Pad | Upper/Right/Left Back Flap | Face Contactors |
| Right/Left Wall | Top Wall | Edge Contactors |
| Right/Left Bottom Flap | Right/Left Wall | Face Contactors |
| Right/Left Bottom Flap | Bottom Wall | Edge Contactors |
| Stomp Pad Bottom | Bottom Wall | Face Contactor |
| Teflon Fabric | Stomp Pad | Face Contactors |
| Environment Nodes | All faces (except back) of MiniShroud | Radiation conductor paths set by view factor |

## C. Boot Model

The thermal model of the xEMU boot was derived from the latest CAD geometry. Figure 4 illustrates the boot's layered configuration as represented in the thermal model, with pink regions indicating thermocouple (TC) locations. Material properties for each layer—such as thermal conductivity, specific heat, and optical characteristics—reflect the actual xEMU boot assembly.

The foot was modeled either as boundary nodes or as a human foot representation. For correlation purposes, boundary nodes were used to match the nearly isothermal condition of the manikin foot during testing. The human foot model accounts for blood, core (bones), muscle, fat, and skin layers but does not resolve spatial temperature variations (e.g., toes, arch, heel), which is identified as future work. Ultimately, for this work, the human foot model was not utilized (details about this are in Section IV).

Each boot layer was thermally coupled to adjacent layers using linear contactors or conductors. Table 2 summarizes critical thermal paths; only those essential to model performance are included. Heat transfer with the environment occurs primarily through two modes: (1) radiation to environment and (2) conduction via the sole tread. Regions insulated with the environmental protection garment (EPG) were modeled with variable effective emissivity, adjusted during correlation. Non-EPG areas such as the outsole radiate based on their optical properties. Contact with the stomp pad was represented by linear contactors at tread tops, with an option for full sole contact—including tread valleys—when simulating walking on regolith.

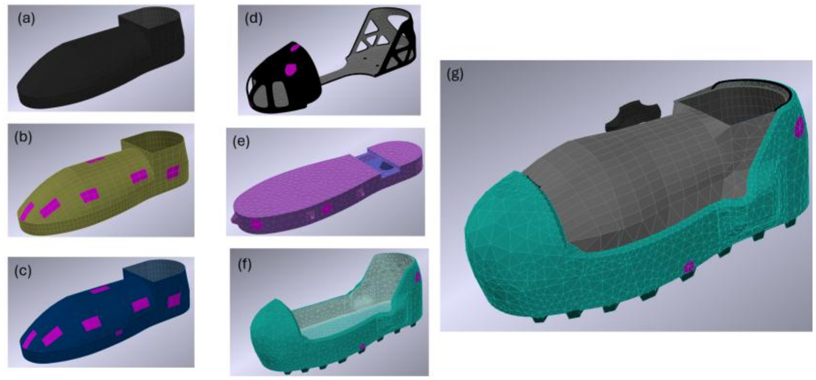


**Figure 4. Thermal Desktop Boot Model: (a) sock, (b) pressure bladder, (c) restraint layer, (d) frame, (e) thermal insert, (f) outsole, and (g) full assembly.**

**Table 2. Critical thermal contacts within Boot Model.**

| From | To | Description |
|---|---|---|
| Upper Foot Node | Sock | Linear Conductor |
| Lower Foot Node | Sock | Linear Conductor |
| Sock | Pressure Bladder | Linear Contactor |
| Pressure Bladder | Restraint | Linear Contactor |
| Restraint | Frame | Linear Contactor |
| Frame | Thermal Insert (Top) | Linear Contactor |
| Thermal Insert (Top) | Thermal Insert (Bottom) | Radiation environment and conduction through material |
| Thermal Insert (Bottom) | Outsole | Linear Contactor |
| Frame | Outsole | Linear Contactor |
| Outsole Bottom | Stomp Pad | Linear Contactor or radiation heat loss |
| Outsole Sides | Environment | Radiation through MLI → effective emissivity |
| Overlayer | Environment | Radiation through MLI → effective emissivity |

## D. Correlation of MiniShroud Model

### *1. Process*

The MiniShroud thermal model was correlated using four steady-state test conditions: two contact cases and two radiation cases, with varying stomp pad temperature set points and ventilation flows through the boot. The initial correlation approach targeted MiniShroud environment coupons and their associated TCs mounted on the shroud wall. However, a lack of clear imagery and documentation prevented accurate three-dimensional placement of these coupons within the thermal model. Consequently, correlation relied on TCs taped directly to the walls, which had photos indicating positioning. Mapping TC locations in the model was simplified by converting oblique photographs into top-down views using a MATLAB-based image transformation workflow (fitgeotrans and imwarp functions) [11] [12]. This process enabled precise (x, y) coordinate extraction for TC placement, which was then linked to corresponding model nodes for temperature readout in Thermal Desktop logic and referenced during SOLVER execution.

The primary method of model correlation was to adjust the portions of the model with the most uncertainty– in this case, the environmental sink temperatures, representing the vacuum chamber space outside the MiniShroud. No TCs were installed in this region; however, chamber shroud wall measurements indicated temperatures near 40 °F, which served as an initial guess for top, bottom, and side sink temperatures. A 70 °F initial guess was applied to the front sink temperature, representing the view to the warm load lock. Additionally, several estimated conduction coefficients significantly influenced shroud temperatures. These were incorporated as design variables in SOLVER and iteratively adjusted until convergence.

The SOLVER functionality in Thermal Desktop was employed to optimize the model. SOLVER iteratively adjusts selected design variables across multiple model runs to minimize an objective function that quantifies correlation accuracy. For this analysis, the objective function was defined as:

$$OBJECT = \sqrt{\sum\left(T_{model,i} - T_{test,i}\right)^2} \quad (2)$$

where $T_{model,i}$ is the model-predicted temperature and $T_{test,i}$ is the corresponding test measurement. Summations were performed over all wall-mounted TCs and across multiple test days. The $OBJECT$ value represents the overall deviation between model predictions and test data, providing a metric for correlation quality. The SOLVER function perturbed design variables until the $OBJECT$ value was minimized. While SOLVER automated much of the process, certain properties—such as optical and thermal characteristics—required manual updates between iterations. Consequently, the correlation workflow remained partially iterative. Figure 5 presents a flowchart summarizing the correlation process. A summary of design variables and their final values is included in Table 3. Contact test points of varying stomp pad temperature set points were correlated separately from each other since environment temperatures are affected by stomp pad temperature. Design variables beginning with "T" represent temperatures of the given location. StompPad2Bottom represents the conduction coefficient from the bottom of the stomp pad to the bottom wall, and FlaptoSideScrew is the conductivity of the screw between the bottom flaps to the sides of the MiniShroud.

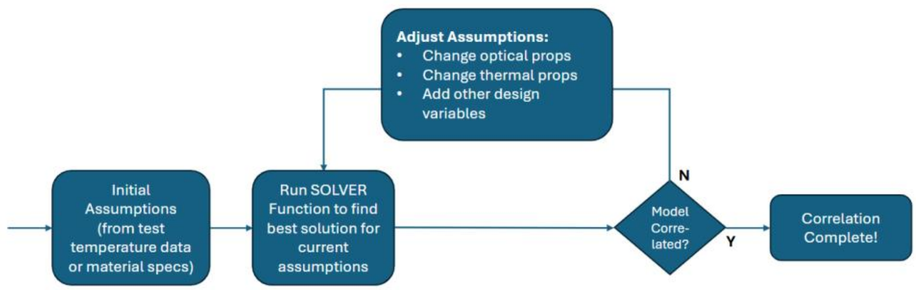


**Figure 5. Environment correlation process.**

*2. Comparison of Correlated Model to Test Data*

The difference between test data and correlated model data is shown in Figure 6. A positive error indicates that the model values are colder than the experiment values. This model was considered correlated because the temperature difference between model and test data did not exceed 8 °C, a small difference given MiniShroud thermal gradients and sensor placement uncertainty. Sensors on the stomp pad and bottom wall exhibited better agreement than those on the side walls.

**Table 3. Optimized parameters for MiniShroud correlation. The minimum temperature boundary set for the SOLVER was 255.4 K (0°F), which was reached by the right side of the chamber.**

| Design Variable | All Radiation Test Points | Contact, 48-60 K setpoint | Contact, 100 K setpoint | Units |
|---|---|---|---|---|
| Tchambersink_floor | 255.8 | 272.0 | 264.2 | K |
| Tchambersink_left | 284.9 | 279.8 | 282.9 | K |
| Tchambersink_right | 255.4 | 255.4 | 255.4 | K |
| Tchambersink_top | 309.1 | 289.2 | 299.2 | K |
| Tload | 292.0 | 294.8 | 294.7 | K |
| StompPad2Bottom | 16.139 | 21.276 | 25.297 | $W/K/m^2$ |
| Flap2SideScrew* | 0.100 | 0.129 | 0.100 | W/K |

*3. Thermal Performance and Temperature Gradients*

Figure 7 shows the MiniShroud chamber temperatures from the Thermal Desktop model. Model units are shown in Fahrenheit, with Celsius equivalents in parentheses. The image emphasizes significant nonuniformity in temperature: the top panel ranges from −189 °C to −142 °C, while the bottom panel reaches −118.4 °C. Located in the back of the shroud and thermally strapped to the copper bars, the stomp pad is even colder. Not shown is the SLI curtain, which approached 0 °C due to heat from the load lock, creating a warmer environment for boot surfaces facing the load lock compared to those facing the chamber sides. It is important to note that the stomp pad also had pieces of Teflon fabric covering the areas not contacted by the boot. This was to reduce shininess from the aluminum stomp pad reflecting into the environment, but this resulted in warmer temperatures on the covered part of the stomp pad surface Future testing will likely remove this and anodize or paint the uncontacted surface to reduce shininess, lowering the internal MiniShroud emissivity.

This nonuniformity underlines the importance of accurate TC node mapping. Performing the MATLAB-based image transformation was necessary to ensure precise TC placement in the model, as large thermal gradients across the walls could otherwise lead to invalid SOLVER results. Greater uniformity could be achieved by increasing MiniShroud wall thickness or cooling the entire chamber to provide a colder, more consistent radiation environment. Future tests should prioritize achieving a uniform, low-temperature radiation environment.

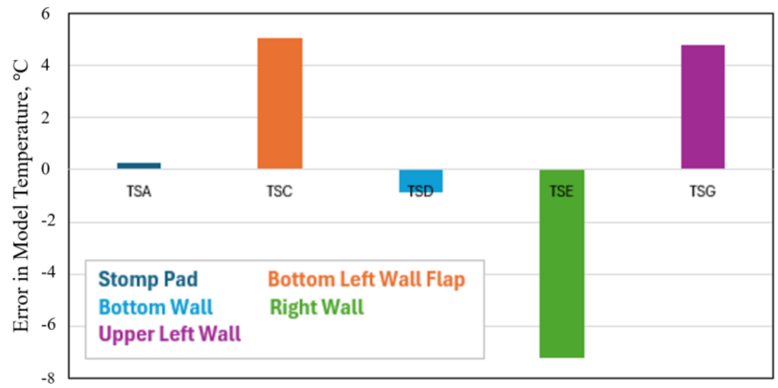


**Figure 6. Temperature difference between test data and correlated model data. Positive values indicate that the model is colder than the test data.**

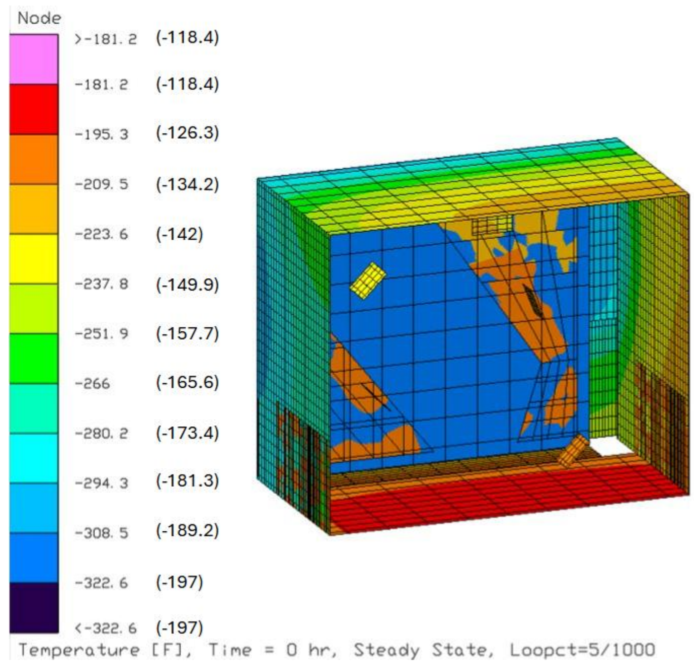


**Figure 7. Internal view of MiniShroud with surface temperatures shown. Values in parenthesis are in °C. Orange and yellow coloration on the stomp pad represents the Teflon fabric cutouts to reduce exposed shiny parts of the aluminum stomp pad.**

## E. Correlation of Boot Model

*1. Process*

The model was correlated to ten steady-state test conditions for varied stomp pad temperature set points, ventilation flowrates and contact configuration (contact with stomp pad vs. radiation only). Because chamber and boot geometry differed between radiation and contact cases (boot positioned closer to the stomp pad during contact), two separate models were correlated—a contact model and a radiation model.

Correlation focused on parameters with the greatest uncertainty, including thermal contactors and conductors between boot layers, thermal and optical properties, and insulation performance. The Thermal Desktop SOLVER function was used to iteratively adjust conductance values to minimize error and improve model correlation. However, the boot model includes numerous variables, and SOLVER performance decreases as the number of design variables increases. To address this, a local sensitivity analysis was performed prior to optimization of the model. Each conductance was varied independently by ±10%, and the model was run twice per variable to quantify its impact on the overall temperature results. Variables with minimal influence were excluded from the correlation process to improve efficiency of the SOLVER. Because correlation is inherently iterative, multiple sensitivity studies were conducted for different configurations.

In addition to identifying the most influential parameters, initial conductance estimates were required. At first, the original model provided initial guesses; however, these were found to produce large discrepancies between test data and model data. To improve accuracy, the thermal resistances calculated from test data (using heat flux measurement from manikin foot and temperature sensors) were used to generate initial conductance values, which is defined as the inverse of thermal resistance.

After establishing critical conduction coefficients and initial estimates, the SOLVER function in Thermal Desktop was again used to optimize the model. For this analysis, the objective function was defined as:

$$OBJECT = \sqrt{\sum\left(T_{model,i} - T_{test,i}\right)^2 + K \cdot \sum\left(q_{model,i} - q_{test,i}\right)^2} \tag{3}$$

where $T_{model,i}$ is the model-computed temperature; $T_{test,i}$ is the test temperature; $K$ is a scaling factor (either 5,000 or 10,000); $q_{model,i}$ is model-computed heat leak from the foot; and $q_{test,i}$ is the heat leak from the foot during testing. The scaling factor adjusts the relative weight of heat leak accuracy versus temperature accuracy of the model. A higher $K$ results in a model with more accurate heat leak computations and less accurate temperature calculations. Summations were performed over all boot thermocouples and multiple test days.

The $OBJECT$ value represents overall correlation quality, and SOLVER perturbs design variables until this metric is minimized. Although SOLVER efficiently iterates on conduction coefficients, other properties—such as emissivity, optical characteristics, and material thermal properties—require manual updates. Consequently, the correlation process remained iterative. Figure 8 illustrates the steps in correlating the boot model.

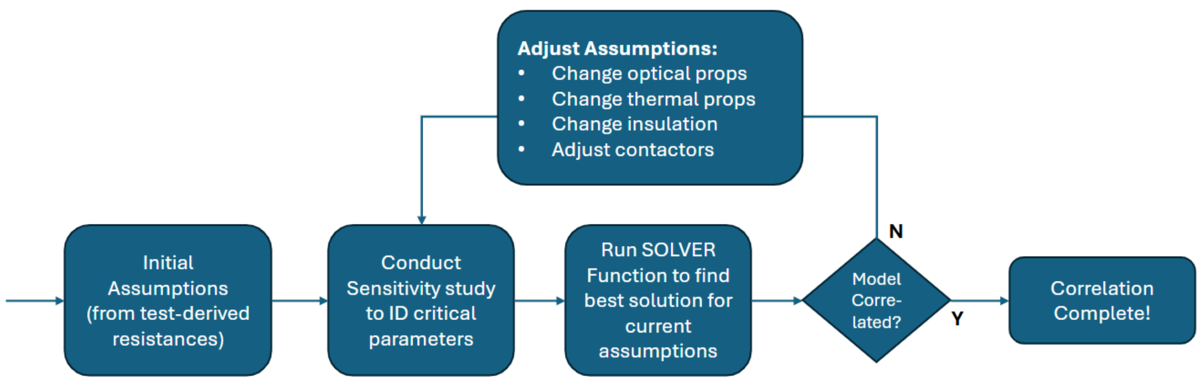


**Figure 8. Boot model correlation process.**

Further complexity arose from varying test conditions. Separate correlations were performed for radiation and contact cases due to geometric differences (boot compression during contact). Flow conditions also influenced internal conduction coefficients within the pressure bladder; therefore, foot-to-sock conduction coefficients were allowed to vary between flow and no-flow cases. Conduction coefficients outside of the pressure bladder (e.g., thermal insert to outsole) were not allowed to change between differing flow conditions. Non-conductor assumptions, such as optical and thermal properties, remained constant across all iterations.

Apart from modifying the conduction coefficients, five key changes to the model were implemented throughout the correlation process.

- The effective emissivity of the EPG increased from 0.06 to 0.10 to reduce the discrepancy of excessive heat loss through the sole predicted by the model versus what was observed experimentally. This higher value, though above typical spacesuit assumptions, could be justified by the complex geometry of coverage and layer compression effects.
- The thermal insert conductivity was decreased by an order of magnitude to account for combined effects of geometry, material properties, multi-layer insulation (MLI) distribution, and dimple contact on heat transfer. This simplification enabled practical correlation, though it may not be completely accurate to the physical

system. Future modeling improvements could better represent the thermal insert and avoid need to adjust conductivity.

- The stomp pad emissivity was increased from 0.2 to 0.5 to correct overly warm outsole temperature predictions. Warm outsole predictions are indicative of an overly high radiative thermal resistance from the outsole to the stomp pad. The emissivity was increased to correct this, and this adjustment can be supported by the Teflon layers (emissivity ~0.9) covering most of the stomp pad surface as well as potential surface degradation from repeated contact during boot installation.
- The contactors between the pressure bladder and restraint were adjusted to represent a toe that does not have perfect contact with the toe of the boot. In contact cases, the restraint and bladder in the toe regions were consistently colder in test than predicted by the model. This was likely due to a higher resistance from the toes to the pressure bladder and restraint.
- Outsole-to-stomp pad conduction was allowed to vary between contact cases to align with TC data. Though this conduction would not normally be expected to change between contact cases, the boot may not have been making perfectly uniform or consistent contact with the stomp pad from case to case. This adjustment was excluded from final performance predictions as its variation is caused by inconsistent test setup rather than boot design.

Table 4 presents the final conduction coefficients for all four conditions. In general, contact cases exhibit slightly higher conduction coefficients than radiation cases, primarily due to compression of boot layers under load. The effect of ventilation flow was limited to the foot-to-sock conductions, which were reduced when flow was off, reflecting decreased convective heat transfer to the pressure bladder. For modeling simplicity, adjustments were applied only to foot-to-sock conduction coefficients rather than foot-to-sock and sock-to-bladder. Since there were no thermocouples installed on the sock or sizing insert, there was no data for this region. From a thermal perspective, these regions behave similarly; however, varying foot-to-sock conduction coefficients provided greater control because they are represented by two discrete conductors (top and bottom), whereas sock-to-bladder conduction applies uniformly around the foot.

**Table 4. Correlated boot model conduction coefficients, W/m$^2$-K.**

| Contactor/Conductor | Radiation, Flow | Radiation, No Flow | Contact, Flow | Contact, No Flow |
|---|---|---|---|---|
| bladder2restraint | 10.397 | 10.397 | 10.851 | 10.851 |
| bladdersoledirect2sock | 141.96 | 141.96 | 141.96 | 141.96 |
| bracket2upperframe | 0.324 | 0.324 | 0.585 | 0.585 |
| dialflap2restraint | 283.91 | 283.91 | 283.91 | 283.91 |
| frame2inserttop | 0.545 | 0.545 | 2.646 | 2.646 |
| frame2outsole | 3.373 | 3.373 | 2.271 | 2.271 |
| frame2restraint | 6.842 | 6.842 | 7.041 | 7.041 |
| framedimple2outsole | 28.391 | 28.391 | 28.391 | 28.391 |
| insert2outsole | 6.899 | 6.899 | 4.713 | 4.713 |
| insertdimples2outsolesides | 0.568 | 0.568 | 0.568 | 0.568 |
| lofoot2losock | 3.623 | 3.878 | 2.958 | 2.862 |
| overlayer2restraint | 283.91 | 283.91 | 283.91 | 283.91 |
| sock2bladder | 283.91 | 283.91 | 283.91 | 283.91 |
| stomppad2outsole | unused | unused | 2.703 | 2.703 |
| upfoot2upsock | 4.276 | 3.833 | 4.032 | 3.697 |

### 2. *Comparison of Correlated Model to Test Data*

Heat leak is a critical parameter as it directly influences boot thermal performance. Figure 9 shows heat leak error by boot region; ankle heat leak is excluded due to limited model fidelity above the ankle. For nearly all test points, the total heat leak error remained below 10%, except for January 30 at the bottom of the foot. The largest discrepancies occurred under radiation conditions without ventilation, likely because only the conduction coefficients affected by flow were adjusted. In general, the model is slightly conservative for contact cases (overpredicting heat leak) and slightly non-conservative for radiation-only test points.

Temperature differences between test data and model predictions for individual TCs were also analyzed across multiple test days. Detailed plots of these comparisons are documented in the test report, an internal NASA document [13]. Most TCs exhibited errors below 10 °C, with only a few exceeding 20 °C. Larger errors generally occurred at sensors farther from the foot, where steep thermal gradients existed due to low-conductivity boot materials. Model accuracy is highly sensitive to TC placement within each layer, and because exact sensor locations could not be verified after boot assembly, potential positional uncertainty exists in these results.

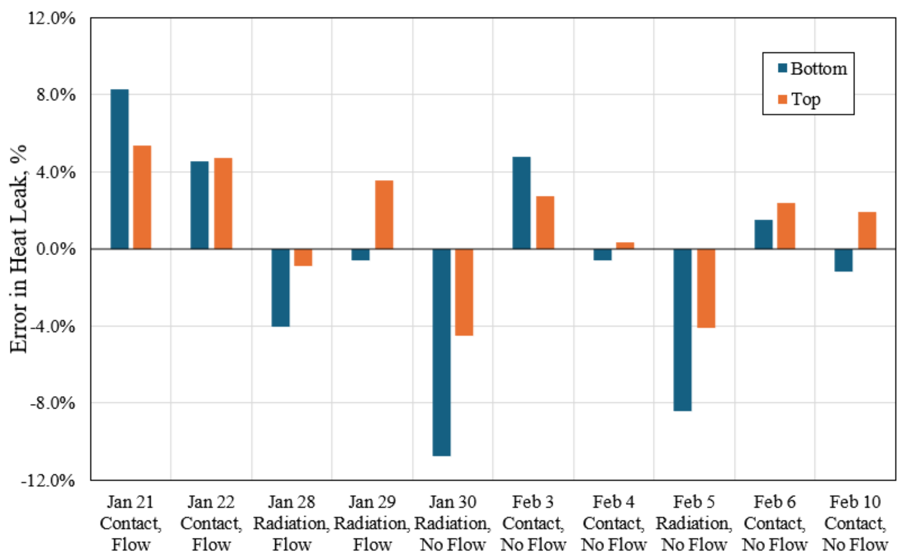

**Figure 9. Error in heat leak for all steady state test days. Positive error indicates a conservative model that predicts more heat leak than was observed during test.**

Sensors with consistently high error included TS-00 (underside of toe in pressure bladder), TS-45 (near the heel on upper frame), TS-59 through TS-64 (outsole), and TS-75 (near heel on EPG). TS-00 is particularly sensitive due to uncertainty in foot positioning and the low conductivity of the bladder. TS-45 and TS-75 were consistently colder in the model, suggesting unmodeled thermal paths near the ankle that may warm the heel during testing, and outsole temperatures were likely highest in error since they were farthest away from the foot with a high thermal gradient. To identify broader trends, TC data were averaged by layer across all test days. This data is shown in Figure 10. A perfectly correlated model would align with the one-to-one ($y = x$) line in this comparison. Each data point represents the average of all temperature sensors on a given layer (indicated by color). The different data points within each color represent the different test days. Data points that fall above the line (model temperature greater than test temperature) are non-conservative. Results show bladder layers closest to the foot split the line, with contact cases generally conservative and radiation cases slightly non-conservative. Additionally, layers above the thermal insert (bladder, restraint, frame) were significantly warmer than layers below (thermal insert and outsole) or outside insulation (EPG), highlighting the effectiveness of the thermal insert and MLI in maintaining foot warmth.

*3. Final Predicted Performance of Boot Model*

Temperature differences between test data and model predictions for directly tested conditions was previously discussed. However, these comparisons do not provide insight into expected performance for untested scenarios. To address this, root-mean-square error ($RMSE$) was computed for each TC across all ten steady-state test days:

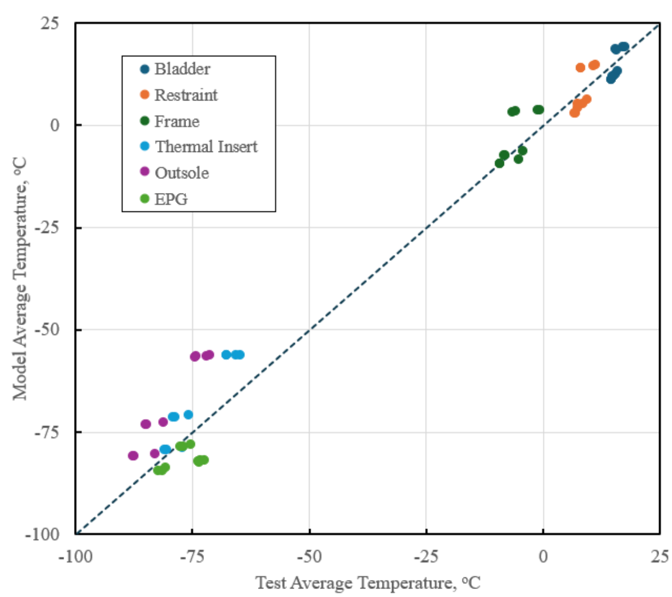

**Figure 10. Comparison of Test vs Modeled Average Layer Temperatures.**

$$RMSE_i = \sqrt{\frac{\sum_{i=1}^{N}(T_{model,i} - T_{test,i})^2}{N}} \quad (4)$$

Where the sum from $i = 1$ to $N$ is the total across the ten test days that were modeled. $RMSE$ serves as a statistical measure of model accuracy and can be used to establish confidence intervals; for example, a 95% confidence interval corresponds to an uncertainty of $2 \cdot RMSE$.

To estimate $RMSE$ for conditions beyond those tested, a statistical method called bootstrapping was applied by resampling (with replacement) from the ten test days. This approach predicts expected $RMSE$ under operational scenarios and quantifies uncertainty. Analysis showed that sensors closest to the foot exhibit the lowest error, while sensors near the outsole and EPG have higher variability due to large thermal gradients and positional uncertainty. Figure 11 plots the average expected $RMSE$ of the model by layer, with a 95% confidence.

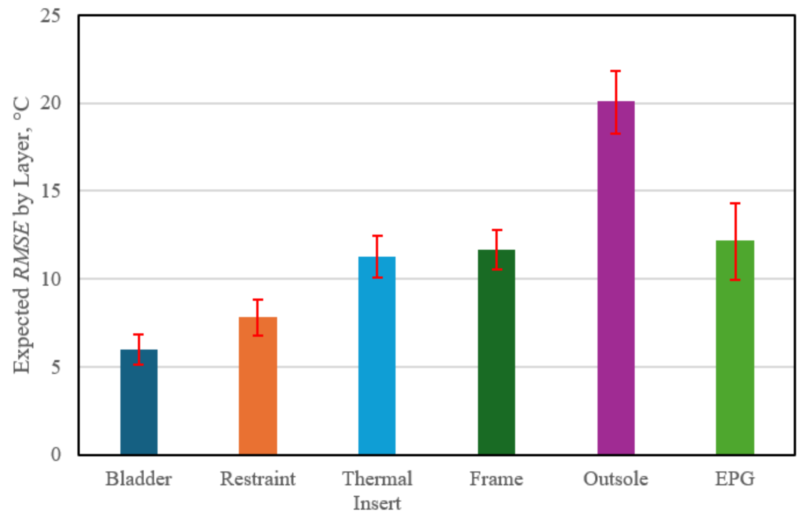


**Figure 11. Expected $RMSE$ (°C) of model by layer. Error bars represent the expected variation of $RMSE$ for any condition based on 95% confidence.**

$RMSE$ was also computed for heat leak. Despite localized temperature errors, heat leak predictions were highly accurate which can be attributed to the deliberate modeling strategy of prioritizing the heat loss correlation accuracy considering its critical role in meeting performance requirements. The results shown in Table 5 indicate strong confidence in heat leak predictions, even under varying conditions. Typical heat leak values for the bottom of the foot and top of the foot were 1.8 W and 2.3 W, respectively. The $RMSE$ statistics presented here are used later to quantify uncertainty in boot performance predictions under operational conditions. One potential drawback of assessing uncertainty using the $RMSE$ is that it may fail to capture the impacts of large gradients and temperature outliers. The error calculation will only be as good as the data that is collected during test. For this reason, future testing of boot designs will emphasize instrumentation in the locations of largest temperature gradients seen from this test series to ensure the gradients can be accurately characterized.

**Table 5. Expected $RMSE$ for heat leak. Error is based on expected variation of $RMSE$ for any condition based on 95% confidence.**

| Location | Expected $RMSE$ (W) | Uncertainty on $RMSE$ (W) |
|---|---|---|
| Bottom of Foot | 0.101 | +0.042 / -0.033 |
| Top of Foot | 0.076 | +0.021 / -0.018 |

*4. Thermal Performance and Temperature Gradients*

The boot model exhibits significant temperature gradients both between and within individual layers. Figure 12 illustrates these gradients across major layers, highlighting the performance of the thermal insert and outsole, which act as effective insulators by maintaining warmer internal conditions despite exposure to extremely cold external environments. The figure also shows localized cooling in the toe region compared to other areas within the same layer. Figure 13 focuses on internal layers such as the sock, pressure bladder, restraint, and frame. Pronounced gradients are evident within these layers, particularly in the restraint and frame, where temperatures near the toe are substantially lower than those beneath the arch. The heel also trends colder, though the outsole provides slightly better insulation in this region than at the toes. These observations emphasize the importance of accounting for localized thermal behavior when evaluating boot performance.

Across layers, extreme gradients exist between the foot (near 300 K) and the contact surface (~50 K). This performance is largely enabled by the thermal insert, which minimizes conduction pathways and incorporates vacuum pockets to reduce heat transfer. The outsole also provides strong thermal resistance, aided by tread geometry that limits conductive paths. Overall, these features allow the boot to maintain a warm internal environment under cold external conditions.

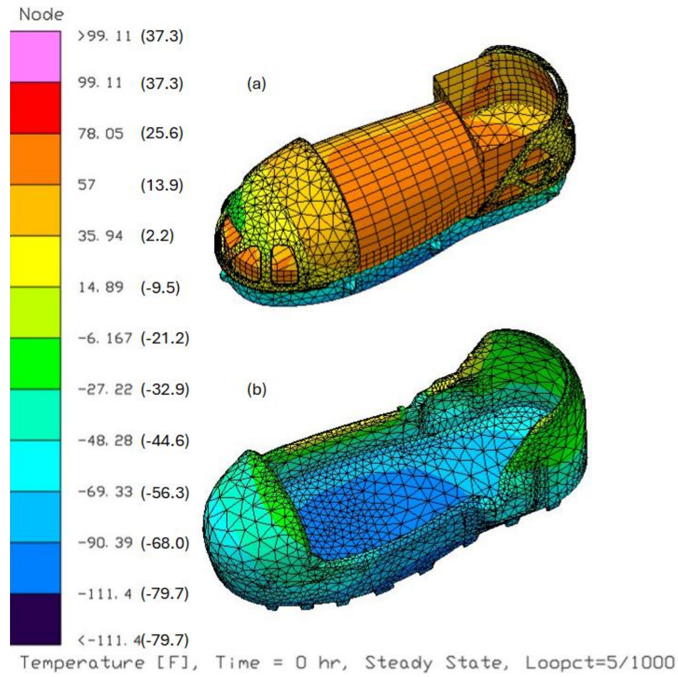

**Figure 12. Radiation case temperature gradients between layers of the boot. (a) restraint, frame, and thermal insert; (b) outsole. Temperatures in Celsius are provided in parentheses.**

## IV. Predicted Performance of Boots in Operation

The ultimate goal of model correlation to test data is to develop an accurate model that can be used to estimate the performance of the boots in operation. This section discusses the predictions of the correlated model for operation in lunar operations. Predicting performance does present some challenges as there is not currently good test data characterizing the conductance between a boot and lunar regolith. Also, a high-fidelity foot model with discretized regions where local gradients may occur, such as the toes, is important for capturing accuracy in boot performance. Other important considerations for model accuracy include dynamic changes during walking such as flexion and compression of different regions over time as steps are taken.

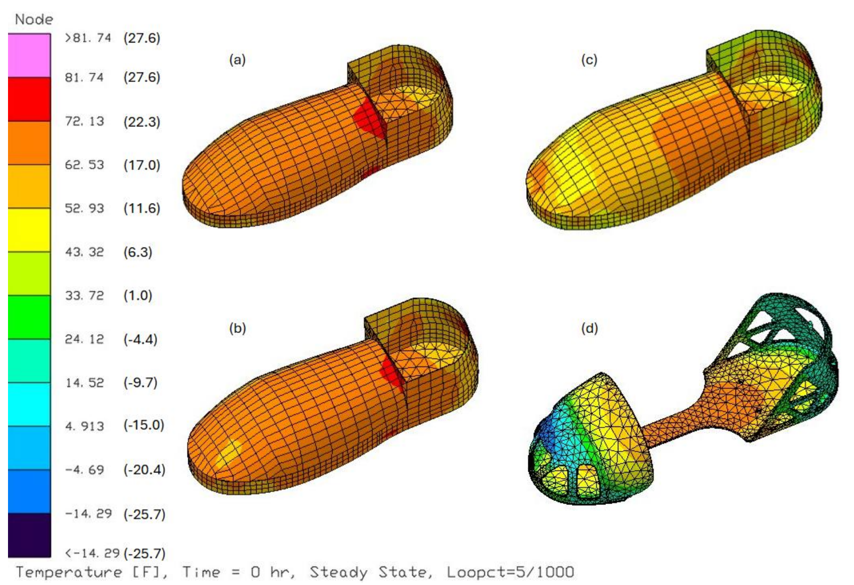

**Figure 13. Radiation case temperature gradients throughout individual layers of the boot. (a) sock, (b) pressure bladder, (c) restraint, (d) frame. Temperature in Celsius are provided in parentheses.**

### A. Required Updates to Model for Lunar Operation Performance

Two major updates were implemented to transition the model from laboratory conditions to lunar operations: adjustments to outsole contact and foot representation.

During testing, the boot contacted a flat stomp pad, whereas on the Moon, the sole will compress into regolith, increasing contact area since tread valleys will be filled. Because no regolith-specific conductance data exists, the per-area conduction coefficient was assumed using the test-derived outsole-to-stomp pad value of 2.703 W/m$^2$/K as an initial estimate. A sensitivity analysis was later performed to evaluate the impact of this assumption.

To model a human foot, two approaches were considered: (1) a constant top and bottom foot temperature, similar to the manikin setup, or (2) a simplified human metabolic foot model dividing the foot into two locations (top and bottom) with a layered representation (blood, core, muscle, fat, and skin) at both locations. This is more analogous to actual performance of a foot in a boot.

The second approach was deemed non-conservative because it does not capture localized gradients—particularly colder toes. A higher-fidelity model discretizing individual toes would require human testing which was not performed at this time. Instead, an intermediate solution was implemented by adding a toe node to the boundary condition model. The updated foot representation included three nodes: upper foot, lower foot (excluding toes), and toes. Toe conductance to the sock was assumed equivalent per unit area to the rest of the foot. Boot performance was assessed by comparing local toe heat flux to permissible limits. This method supports steady-state analysis only; transient predictions would require an advanced foot model tied to human test data.

### B. Permissible Heat Flux

Because the model cannot resolve individual foot layers, permissible heat flux limits were derived to assess boot performance. Previous EMU glove testing incorporated a high-fidelity hand model correlated to human data, which resolved palm, fingers, and fingertips [14], [15]. While not perfectly analogous, this model provides insight into heat flux thresholds for maintaining skin temperature. The thumb tip, similar in geometry to a toe, was used to establish a relationship between heat flux and skin temperature.

NASA-STD-3001 specifies a minimum skin temperature of 15 °C (59 °F) [16], while historical boot requirements used 10 °C (50 °F). To address both limits, analysis was performed for 10 °C and 15 °C thresholds. Interpolation of glove model data indicates maximum heat flux requirements of approximately 120.8 W/m² (38.3 Btu/hr/ft²) for 10 °C and 111.4 W/m² (35.3 Btu/hr/ft²) for 15 °C. Previous boot analyses assumed a permissible heat leak of 9.7 W (≈170.5 W/m²) based on the Wissler metabolic model, which does not discretize toe regions and is therefore non-conservative [9]. These findings confirm that glove-derived values are within the correct order of magnitude while providing a more conservative basis for evaluation (lower permissible heat flux).

### C. Expected Performance of Boot in PSR Conditions

#### *1. Heat Flux*

Heat flux at the toe was evaluated for varying environment temperatures between 48 K and 120 K and outsole-to-regolith contact conduction between 0.24 Btu/hr/ft$^2$/°F (1.36 W/m$^2$/K) and 159.2 Btu/hr/ft$^2$/°F (904 W/m$^2$/K), assuming foot temperatures of 10 °C (50 °F) and 15 °C (59 °F), such that the heat leak calculated would model the heat leaving the toes when the skin temperature limit is reached. The results from this study are shown in Figure 14 and indicate strong sensitivity to contact conduction, where small variations significantly affect heat flux and could determine pass/fail outcomes. When a 10 °C skin temperature limit is assumed (max heat flux of 111.4 W/m$^2$), the minimum permissible temperature is at or below 100 K for most conductances. This means it is likely that the boot will be keep the crewmember safe for 8 hours down to 100 K, which is the 8 hours requirement on the boots. Unfortunately the permissible temperature is above the 2 hour requirement of 48 K for many assumed conductances so it is inconclusive if the boot can maintain operation at 48 K in a steady state condition. For the 15 °C skin temperature limit, performance at 100 K became marginal, and continuous operation at 48 K was not feasible for any conductance. Determining allowable exposure time at 48 K would require transient analysis, which was not performed due to the absence of a high-fidelity foot model.

To quantify uncertainty in these results, a Monte Carlo simulation was performed using bootstrapped $RMSE$ values from model correlation (heat flux $RMSE$ of about 4.44 W/m²). Each test point was sampled 100,000 times, assuming a normal error distribution, and permissible

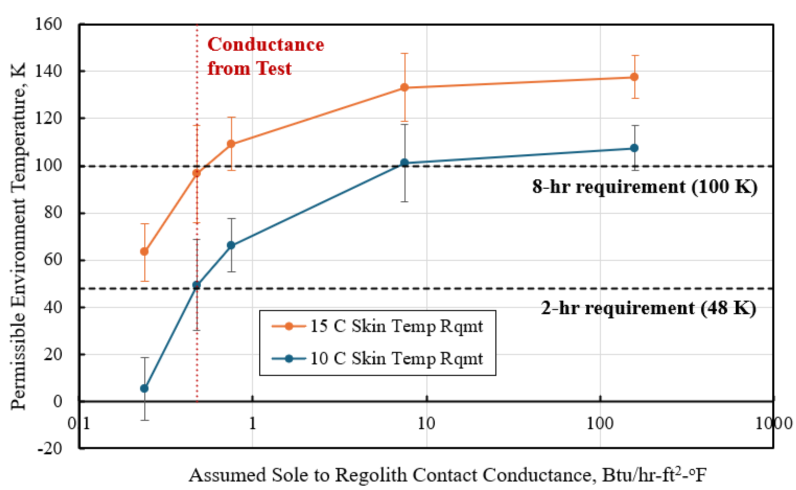


**Figure 14. Minimum permissible environment temperature for continuous operation with model uncertainty. Error bars represent the standard error for the model, as computer using a Monte Carlo Simulation.**

temperatures were computed for each iteration. The resulting uncertainty bands signify that, despite accurate heat flux predictions, permissible temperature estimates remain highly sensitive to model uncertainty. Reducing these uncertainties would require improved correlation or a more detailed foot model to mitigate sensitivity to small heat flux variations.

*2. Temperatures*

In addition to estimating the expected heat flux during lunar operations, the minimum temperatures across various boot layers were also computed. These calculations assumed a constant foot temperature of 10 °C, representing the coldest possible boot conditions. Two primary sources of uncertainty were addressed: (1) contact conductance between the regolith and outsole, and (2) inherent model uncertainty. To quantify the impact of contact conductance, a temperature range was derived from parametric results using conductance values of 0.24 Btu/hr/ft²/°F (1.36 $W/m^2/K$) and 159.2 Btu/hr/ft²/°F (904 $W/m^2/K$). Model uncertainty is incorporated by adding the $RMSE$ error to this range; for a 95% confidence interval, this contribution is twice the $RMSE$. These results are provided in Table 6.

Results indicate that the bladder remains above its minimum allowable temperature in a 100 K environment. At 48 K, the bladder temperature may fall below the limit; however, this risk is minimal because these values represent steady-state conditions, and reaching such temperatures would likely require more than two hours. Temperature ranges for all layers are relatively large, primarily due to uncertainty in contact conductance. Additional testing to better characterize regolith-to-outsole conductance could significantly reduce these ranges. Eliminating conductance uncertainty would reduce error bars in the bladder from ±16 °C to ±13.7 °C; the upper frame from ±36 °C to ±25 °C; and the outsole from ±34 °C to ±27.7 °C. Further refinement of model correlation with emphasis on certain relevant temperatures could also reduce uncertainty and error in those predicted temperatures. Additionally, narrowing the confidence interval would substantially decrease uncertainty.

**Table 6. Minimum expected temperature. Range is based on uncertainty in contact conductance with regolith and model accuracy**

| Layer | Minimum Permissible Temperature | Minimum Expected Temperature at 48 K (with 95% confidence) | Minimum Expected Temperature at 100 K (with 95% confidence) |
|---|---|---|---|
| Bladder | -34.4 °C | -37.2 to -5.0 °C | -34.0 to -3.3 °C |
| Upper Frame | N/A | -109.0 to -37.0 °C | -96.6 to -30.2 °C |
| Outsole | N/A | -225.2 to -157.7 °C | -173.2 to -126.4 °C |

## V. Conclusion

A major outcome of this test series was the successful correlation of the lunar boot thermal model using extensive, repeatable, steady-state data collected under controlled conditions. The model was validated against ten test points, including scenarios with and without outsole contact and ventilation flow, achieving heat leak predictions within 0.1 W accuracy. Statistical methods such as bootstrapping and Monte Carlo simulations were employed to quantify uncertainty, not only for the test conditions but also for operational scenarios. This analysis identified outsole-to-regolith contact conductance as the dominant source of variability, and parametric studies were used to bound its impact on predicted temperatures. The correlated model enabled characterization of permissible environmental temperatures for steady-state operation and provided confidence intervals for performance predictions. Future work should focus on reducing uncertainty through improved regolith contact fidelity, colder and more uniform radiation environments, and enhanced human-in-the-loop foot models for transient analysis. These are all areas that should be addressed as they can greatly influence the predicted performance of the boot in lunar PSRs. Performing this additional work in the future would further refine thermal predictions and strengthen the reliability of EVA boot performance assessments for Artemis missions.

## Acknowledgements

The authors would like to acknowledge the CITADEL test team at JPL for their hard work conducting test points and compiling data files. The authors would also like to acknowledge the use of the AI Microsoft 365 Copilot tool for some of the content presented in Sections II-V. This paper is based on work presented in NASA document CTSD-ADV-2272. Copilot was used to summarize, clarify, and condense the most relevant information about model correlation from that document to fit within 15 pages. All AI outputs were checked for accuracy and edited. AI was *not* used for generation of the figures in this document.

## References


[1] B. Swartout, "xEMU Spacesuit Boot Lunar South Pole Thermal Vacuum Testing," in *International Conference of Environmental System*, Rio Grande, Puerto Rico, 2026.

[2] B. Swartout, "Exploration Extravehicular Mobility Unit (xEMU) Lunar Boot Chamber B Thermal Vacuum Testing Results," in *International Conference on Environmental Systems*, Louisville, 2024.

[3] B. C. Conger, "Thermal Analysis of the EMU Boot with Foam Insert Removed," CTSD 1404, 1992.

[4] T. Durrant, "Orlan Spacesuit Boot Thermal Model," HDID-2G41-1132, 1999.

[5] J. V. Iovine, "EMU Boot Thermal Analysis for ISS EVA," HDID-2G41-954, 1998.

[6] J. V. Iovine, "Thermal Analysis of the EMU Boot Pressure Bladder," CTSD862, 1990.

[7] W. Lee, "Thermal Analysis Results of Stand-Alone Shuttle Boot Model for the Thermal Vacuum Chamber B Test for STS-37 Mission Hardware," CTSD454, 1989.

[8] T. Nguyen, "The Thermal Effect of a Newly DEsigned Aluminum Piece Attached to the Heel of the EMU Boot," 20977, 1984.

[9] D. Ochoa, "Thermal Design and Analysis of Constellation Space Suit System Boot Options for Lunar Missions," ESCG-4470-09-TEAN-DOC-0110, 2009.

[10] D. G. Gilmore, Spacecraft Thermal Control Handbook: Volume 1: Fundamental Technologies, The Aerospace Press, 2002.

[11] "fitgeotrans," Mathworks, [Online]. Available: https://www.mathworks.com/help/images/ref/fitgeotrans.html.

[12] "imwarp," Mathworks, [Online]. Available: https://www.mathworks.com/help/images/ref/imwarp.html.

[13] Z. Fester, S. McFarland, N. Andersen, E. Quick, D. Green, T. Jaimes and D. Morris, "xEMU Boot TVAC Final Report," NASA, CTSD-ADV-2272.

[14] N. L. Langston and V. Margiott, "EMU Phase VI Glove Thermal Vacuum Test and Analysis Final Report," CTSD-SS-1621, 1998.

[15] M. B. Abney, R. J. Jones, S. R. Wilson, T. K. Brady and N. L. Andersen, "Lunar Glove Thermal and Durability Analysis, Test, and Failure Mitigation," NESC-RP-21-01722, 2024.

[16] NASA, "NASA Spaceflight Human-System Standard Volume 1, Crew Health," 2023.